Elasticity and anelasticity of oxide glasses

*E. Courtens, M. Foret, B. Rufflé & R. Vacher**

Groupe de Physique des Verres et Spectroscopies, LCVN, UMR 5587 CNRS, Université Montpellier II, F-34095 Montpellier Cedex 5, France

Manuscript received 6 December 2006
Accepted 24 January 2007

The current understanding of sound properties in glasses is reviewed and compared to that in crystals. Sound damping in oxide glasses is controlled mainly by three processes which in increasing order of the frequency at which they dominate are: the thermal relaxation of defects, relaxation via anharmonic interactions with the thermal bath, and hybridization with optic-like vibrations. The former two also affect distinctly the velocity of sound. The latter one relates to the boson peak and the low temperature plateau generally observed in the thermal conductivity. In addition, in silica and other tetrahedrally coordinated glasses, the sound velocity tends to increase with temperature, presumably owing to a progressive structural change.

I. Introduction

Sound in glasses is a subject which, in spite of its long history, remains of much actuality and activity. Contrary to high quality insulating crystals, many different mechanisms do affect sound velocity and attenuation in insulating glasses, particularly in oxide ones. The purpose of the present paper is to review in simple terms recent progress that has been achieved in the understanding of the frequency and temperature dependencies of acoustic properties in some important model glasses, such as silica.

In single crystals, the main damping mechanism is anharmonicity of thermal atomic vibrations, which results from the interaction of sound with the high frequency vibrational modes constituting the thermal bath.[1] Although often forgotten, the same mechanism also should be active in glasses.[2,3] However, in addition, there is in glasses the interaction of sound with local entities, often called "defects", although the definition of what forms a defect in a disordered system is not necessarily clear. It is the latter that dominates sound *attenuation* at low and intermediate frequencies, up to fairly high ones, often in the gigahertz (GHz) range.[4,5] On the other hand, anharmonicity affects in a major manner the sound *velocity* in the same temperature and frequency regions in many glasses,[2] and this has obscured the comparative understanding of sound velocity and attenuation in such cases.

In this paper we use T for the temperature, Ω for the frequency of specific modes, v for the sound velocity, and α for the energy damping constant, so that $\alpha=l^{-1}$ where l is the energy mean free path. At sonic and ultrasonic frequencies there are several well established methods to determine v and α, although obtaining accurately the absolute value of α might be a delicate point. At hypersonic frequencies, typically in the range of several ten GHz, and in sufficiently transparent glasses, one uses Brillouin light scattering (BLS). In that case, the scattering geometry fixes a scattering vector whose length is given by $4\pi n\sin\theta/\lambda$, where n is the refractive index, θ is the angle between the incident and the scattered light directions, and λ is the light wavelength in vacuum. For reasons of momentum conservation, the scattering vector is also the wavevector q of the observed sound wave, with $q=2\pi/\lambda_s$, where λ_s is the sound wavelength. The spectroscopy measures the frequency Ω of the sound wave, which relates to v by $v=\Omega/q$. The Brillouin signal also has a frequency width Γ (the full width at half maximum, expressed in angular frequencies, just like Ω). This width relates to l^{-1} by $l^{-1}=2\Gamma/v$. It also gives the quality factor of the related harmonic oscillator, $Q=\Omega/\Gamma$, and thus the damping constant is proportional to the internal friction $Q^{-1}=\Gamma/\Omega$, a form that will be used in this paper. It is a merit of BLS that Q^{-1} can be determined with high accuracy in the same experiment that gives $\Omega(q)$. To obtain information at higher frequencies Ω, one might envisage BLS at shorter excitation wavelengths λ. This can be done to some extent using excitation with UV light,[6,7] as long as the samples are sufficiently transparent.[8] At still higher frequencies the samples strongly absorb, until one

* Corresponding author. Email rene.vacher@univ-montp2.fr
Paper presented at the Eigth European Society of Glass Science and Technology Conference, Sunderland, UK 10–14 September 2006

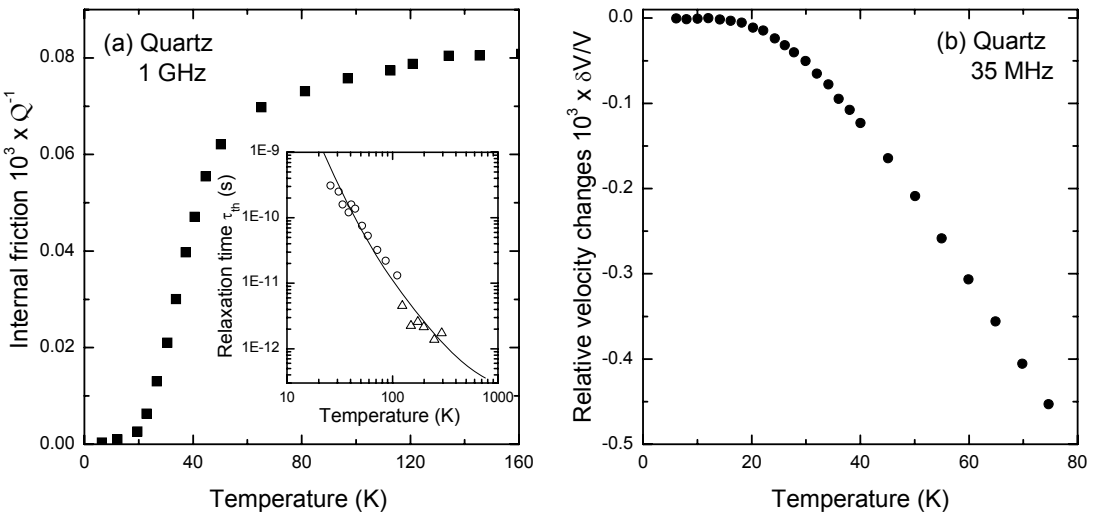

Figure 1. The internal friction (a) of shear waves at 1 GHz in X-cut crystal quartz from Ref. 14. The velocity changes (b) at 35 MHz are taken from an ultrasonic measurement in Ref. 15. The inset in (a) shows the thermal relaxation time τ_{th} from Ref. 16. It should be noted that the line is not a fit through the data points explained in Ref. 16, but an independent theoretical determination calculated from the thermal conductivity

reaches the x-ray region where they become again transparent. The latter has allowed determination of sound frequencies in the terahertz (THz) range using a Brillouin spectroscopy known as inelastic x-ray scattering (IXS).[9] In the difficult frequency region between ~50 GHz and ~1 THz, there exists but a single spectroscopy, known as the picosecond optical technique (POT).[10] This delicate technique is essentially based on the observation of the time-of-flight and decay of a picosecond thermal pulse propagating through a thin glass film.

Sound at THz frequencies is of considerable interest as it controls the thermal conductivity $\kappa(T)$ at low temperatures T. In glasses around 1 K, $\kappa(T)$ grows approximately with T^2, reaching a plateau centred at T_p~10 K.[11] This plateau typically extends over several kelvins, beyond which κ starts increasing again. Below T_p, κ results from the transport of energy by propagating acoustic waves, the phonons, associated with the thermal motion of the atoms. These phonons are excited over a range of frequencies. As T increases, this range broadens. The frequency for the most efficient transport by waves – the dominant excitations – is given by $\Omega \approx 5k_B T/\hbar$, where k_B and $\hbar$ are the Boltzmann and Planck constants, respectively.[12] For $T=T_p$ ~10 K, this relation gives $\Omega/2\pi$ ~1 THz. Hence, the properties of sound at these extremely high frequencies are of direct relevance to κ. The existence of the plateau indicates a fundamental change in the nature of the dominant excitations.

The remainder of the paper will be as follows. In Section 2 we explain in detail the position of the problem, pointing out clearly the strong differences between crystals and glasses for what $v(\Omega,T)$ and $Q^{-1}(\Omega,T)$ are concerned. In Section 3, the damping produced by the thermally activated relaxation (TAR) of defects is discussed. It is shown that this dominates Q^{-1} at low and intermediate frequencies, this over a range of T that can reach up to room temperature. On the other hand, this is not true for v, in which case the influence of anharmonicity is generally relatively strong. In Section 4, we discuss a velocity anomaly of silica and the high frequency end of sound waves. Indeed, in addition to the contributions of anharmonicity and TAR, we find in silica a sizeable contribution to the T-dependence of v which must arise from structural modifications. We also return to the origin of the plateau in $\kappa(T)$ and show that it relates to an observed crossover in the fundamental behavior of sound, from propagating waves at low Ω to diffusive excitations at high Ω. The main points are summarised in the Conclusion.

2. Position of the problem

2.1 Anharmonicity effects on sound waves in crystals

In non-defective large insulating crystals the sole mechanism for sound attenuation is the anharmonic interaction with the phonon bath. In the Akhiezer description,[13] one assumes that T is sufficiently high for the bath to be appreciably populated. The sound wave of frequency Ω perturbs the equilibrium as its associated strain e modifies the frequencies ω_i of the thermal phonon modes by $\gamma_i = \partial \ln \omega_i / \partial e$. The latter can be parametrised by a Grüneisen constant[12] $\gamma = \langle \gamma_i \rangle$, where the brackets designate a suitable average over the population. The perturbed thermal bath relaxes towards its new equilibrium via anharmonic interactions, with a characteristic time τ_{th}. In doing so, it dissipates the energy of the sound wave, and this relaxation is most efficient for $\Omega\tau_{th}=1$. This leads

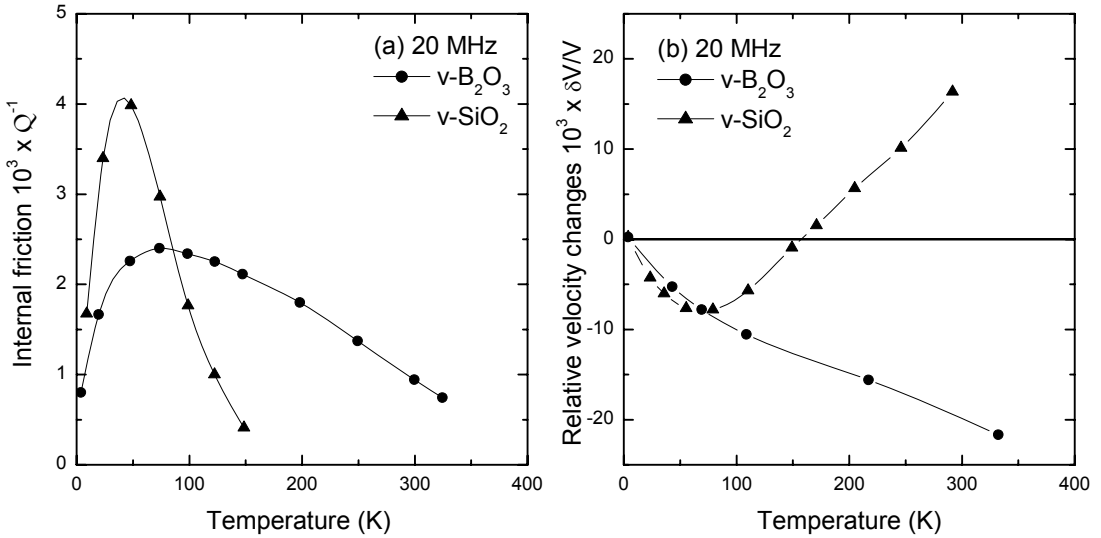

Figure 2. Internal friction (a) and velocity changes (b) measured at 20 MHz in vitreous boron oxide and vitreous silica[18]

to the internal friction[1]

$$Q^{-1}(\Omega,T)=A\Omega\tau_{th}/(1+\Omega^2\tau_{th}^2) \quad (1)$$

As $\tau_{th}(T)$ is generally short, and decreases rapidly with T, the effect on damping is best seen at high Ω and low T where $\alpha \propto \Omega^2$. It can be shown [1] that in this approximation

$$A=\gamma^2 C_V T v/2\rho v_D^3 \quad (2)$$

where C_V is the specific heat per unit volume, ρ is the mass density, and v_D is the Debye velocity defined by $3/v_D^3=1/v_L^3+2/v_T^3$, where v_L and v_T are the longitudinal and transverse sound velocities, respectively.

As a practical example, we consider in Figure 1 the case of crystal quartz, q-SiO_2. We select this crystal as the material is of direct interest for silica glass. Also, the determination of Q^{-1} in q-SiO_2 is a historical experiment, the very first of its kind.[14] Indeed, τ_{th} being so short, the observation of a measurable damping requires experimenting at high Ω. Figure 1(a) shows the value of Q^{-1} obtained at 1 GHz. The increase with T at low T is mostly controlled by the rapid increase of $A \propto T^4$, since $C_V \propto T^3$.[12] Hence, the knee in the curve around 40 K occurs in a region where τ_{th} has already decreased much below Ω^{-1}. In the inset, the values of τ_{th} taken from Ref. 16 are presented. They illustrate this point.

The frequency dependence of the sound damping automatically implies a frequency dependence of the velocity. The Kramers–Kronig transform[17] gives

$$-2\delta v(\Omega,T)/v=A/(1+\Omega^2\tau_{th}^2) \quad (3)$$

In this relation, $\delta v=v-v_\infty$, where $v_\infty(T)=v(\Omega\to\infty,T)$ is the high frequency limit of v. In a crystal, one expects that v_∞ is constant in T, and it can be taken as the low T limit of the measured velocity. For $\Omega\tau_{th}\ll 1$, which is the case in ultrasonics, one simply has $\delta v(T)/v=-A/2$. This produces the T-dependence of $\delta v/v$ illustrated in Figure 1(b). One should note that for small $\Omega\tau_{th}$, $Q^{-1}=A\Omega\tau_{th}$ is small compared to A, whereas $\delta v/v=-A/2$ is Ω-independent. Hence, for increasing Ω an effect is seen on the velocity much before it can be observed on the damping. The reason is that the velocity integrates over all modes with $\tau_{th}<\Omega^{-1}$.

In glasses, even if very high frequency plane waves might not exist, there is thermal agitation, and correspondingly there are populated vibrational excitations. Hence, a mechanism of sound damping similar to the Akhiezer one ought to exist, as discussed below.

2.2 Attenuation and velocity in glasses

Figure 2 shows two examples of internal friction and velocity changes in oxide glasses. It is evident that the behavior pictured in Figure 2(a) is very different from that of Figure 1(a). First, Q^{-1} in glasses is orders of magnitude larger than in q-SiO_2, especially so when one accounts for the fact that the data of Figure 1(a) are taken at a frequency which is 50 times larger than in Figure 2(a). Also the shapes of the signal are very different. It is clear that the signatures in Figure 2(a) should be assigned to another mechanism. This will be explained in Section 3.

On the other hand the decays of $\delta v/v$ at sufficiently high T in q-SiO_2 (Figure 1(b)) and B_2O_3 (Figure 2(b)) are qualitatively similar. It was already recognised long ago that velocity changes in several glasses are dominated by anharmonicity.[2,3] However, there is a strong difference between Figures 1(b) and 2(b) at low temperatures. While in q-SiO_2 the onset is $\propto T^4$, in the glasses it is much more abrupt, apparently $\propto T$. This difference, of course, arises from the very contribution that leads to the peaks in Figure 2(a), and it is given by the Kramers–Kronig transformation

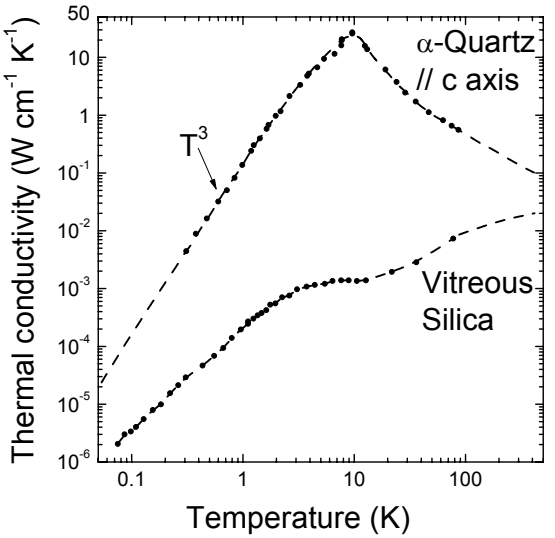

Figure 3. The thermal conductivity of quartz, q-SiO_2, and vitreous silica, v-SiO_2, after Ref. 11

as explained in the following Section. In addition, in vitreous silica, v-SiO_2, the slope in T in Figure 2(b) has the wrong sign. This anomaly is specific to tetrahedrally coordinated glasses.[18] As discussed in Section 4, it suggests progressive structural changes with increasing T.

2.3 Thermal conductivities

It is also of interest, for reasons briefly explained in the Introduction, to compare the thermal conductivities of glasses and crystals. Figure 3 reproduces a well known result.[11]

In q-SiO_2, κ first raises in T^3. The kinetic theory predicts that $\kappa = \frac{1}{3} C_V v_D l_{th}$, where l_{th} is an average mean free path of the thermal phonons.[12] The observed T^3 law corresponds to the Casimir regime where l_{th} is either the size of the sample or the mean distance between sound scattering defects. In that case l_{th} is constant and the T^3 law reflects the T-dependence of C_V. Above this peak, κ decreases strongly owing to anharmonic effects, in which case $\kappa = \frac{1}{3} C_V v_D^2 \tau_{th}$. It is that expression which produces the solid line in the inset of Figure 1(a), in remarkable agreement with the observed data points.[16]

In v-SiO_2, and more generally in glasses, κ is orders of magnitude smaller than in the corresponding crystal. The straightforward kinetic expression for κ is also not valid. Below the plateau, the modes that contribute to C_V are to a large extent non-propagative (the two-level systems), and thus do not contribute to κ. The interaction of the thermal phonons with these two level systems limits their mean free path l_{th}. A modified kinetic expression, restricted to the appropriate specific heat, is still usable. Near and above the plateau, the dominant thermal phonons cease to be propagative plane waves. In that case, the kinetic expresion cannot be used at all to estimate κ.

3. Thermally activated relaxation versus anharmonicity

Figure 4(a) represents schematically a network glass, such as silica.[5] Owing to disorder, several atoms or groups of atoms can occupy two or more equilibrium positions. The displacements indicated by the letters A, B, C (or more complex ones) rather than being harmonic modes could correspond, at defect sites, to double well potentials as shown in Figure 4(b). Owing to disorder, the potential barrier heights V and the asymmetries are distributed according to a probability $P(\Delta,V)$ whose integral is the density of

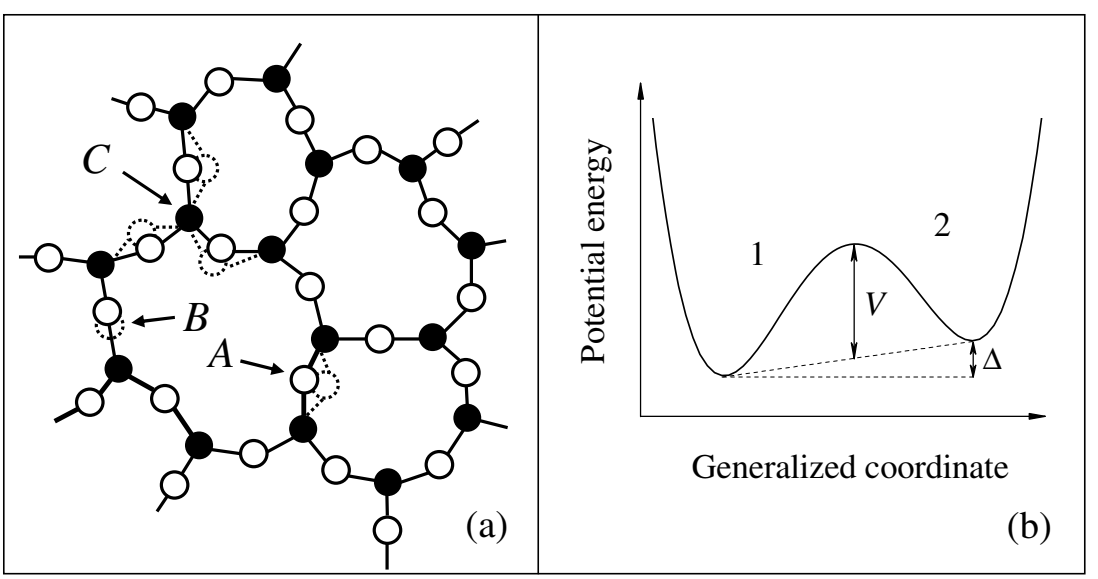

Figure 4. (a) Schematic presentation of relaxing defects, after Ref. 5; (b) a resulting double well potential with the definitions of the barrier height V *and asymmetry* Δ

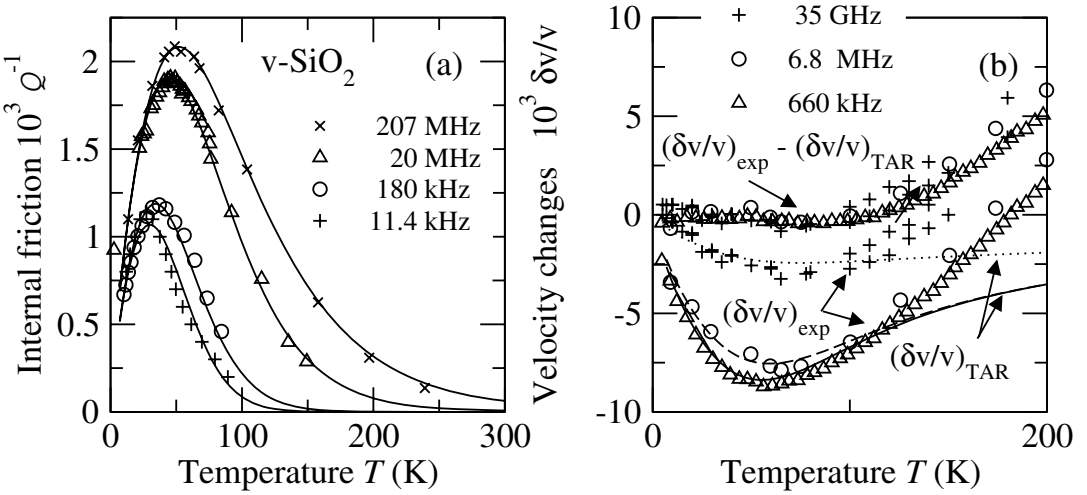

Figure 5. Internal friction (a) and velocity changes (b) in vitreous silica at sonic and ultrasonic frequencies from Ref. 16, where references to the various curves are found. The lines are calculated using TAR with the distribution $P(\Delta,V)$ *explained in the text. The good agreement with the damping data in (a) is striking. TAR also properly accounts for the dip in δv/v as seen in (b), including for the hypersonic result obtained on the longitudinal acoustic mode at 35 GHz. This is emphasised by the curves marked* $(\delta v/v)_{exp}$–$(\delta v/v)_{TAR}$ *which all start with an horizontal tangent at low T*

defects. On the average, the defect population is in equilibrium according to detailed balance: an equal number of defects jumps from 1 to 2 and from 2 to 1 within a given time. The thermal rate of jumping for a given defect is easily calculated to be[19]

$$\tau^{-1} = \frac{1}{2}\tau_0^{-1}\left(\exp\frac{-V-\Delta/2}{T} + \exp\frac{-V+\Delta/2}{T}\right) \qquad (4)$$

where the energies V and Δ are in temperature units, and τ_0^{-1} is an attempt frequency. The inverse rate, τ, is the relaxation time of the defect.

Similarly to the description of anharmonicity in Section 2.1, the sound wave couples to the defects, here by a deformation potential $\gamma=\frac{1}{2}\partial\Delta/\partial e$, modifying their equilibrium population.[19–21] The defects relax towards equilibrium, each with its relaxation time. This leads to an expression very similar to Equation (1), for each single defect, and integrating over the distribution one obtains

$$Q_{TAR}^{-1} = \frac{\gamma^2}{\rho v^2 T}\int_{-\infty}^{\infty} d\Delta \int_0^{\infty} dV P(\Delta,V)\,\mathrm{sech}^2\frac{\Delta}{2T}\left(\frac{\Omega\tau}{1+\Omega^2\tau^2}\right) \qquad (5)$$

The $\mathrm{sech}^2\Delta/2T$ factor essentially has a similar origin as C_V in Equation (2). Details are found in Refs 16, 19.

Of course, owing to the Kramers–Kronig relation examplified by Equations (1) and (3), the velocity changes $(\delta v/v)_{TAR}$ are expressed by an integral similar to Equation (5), in which the last factor within parentheses is replaced by $-1/[2(1+\Omega^2\tau^2)]$. Similarly to the discussion at the end of Section 2.1, one should remark that Q_{TAR}^{-1} is mostly sensitive to those defects for which $\tau=\Omega^{-1}$, whereas $(\delta v/v)_{TAR}$ feels all defects with $\tau<\Omega^{-1}$. Hence, while Q_{TAR}^{-1} is more sensitive to a restricted part of the distribution $P(\Delta,V)$, $(\delta v/v)_{TAR}$ largely integrates over it.

An example of this property is illustrated in Figure 5 which shows sonic and ultrasonic acoustic results on vitreous silica, v-SiO_2. To adjust the experimental data to the above expression one needs a form for $P(\Delta,V)$. We have used[16] a product of two distribution functions, a gaussian in Δ, $f(\Delta)\propto\exp(-\frac{1}{2}2\Delta^2/\Delta_c^2)$, of width Δ_c, times a modified gaussian,[22] $g(V)\propto(V/V_0)^{-1/4}\exp(-\frac{1}{2}V^2/V_0^2)$, of width V_0. The set of parameters (Δ_c, V_0, τ_0) cannot be determined on the basis of Q_{TAR}^{-1} alone. However, if one attempts adjusting simultaneously Q^{-1} and the low-T region of $\delta v/v$ using TAR, one is then forced to restrict the spread in Δ much more than that in V. We found for silica $V_0/\Delta_c=8{\cdot}2\pm0{\cdot}6$, with $V_0=659\pm19$ K and $\log_{10}\tau_0=-12{\cdot}2\pm0{\cdot}18$. This produces the lines through the data points in Figure 5(a). In Figure 5(b), it gives the two lines marked $(\delta v/v)_{TAR}$, which can be subtracted from the experimental $\delta v/v$, showing that TAR effectively accounts for the dip below ~100 K. The remaining velocity changes will be explained in Section 4.

One important result of the above analysis is that while $V_0\approx660$ K, Δ_c is only ≈80 K. This is an interesting structural property. Consider fairly local defects like A or B in Figure 4(a). V_0 is mainly a property of nearest neighbors, and it can be quite large, up to values that are of an order similar to the glass transition temperature T_g. On the other hand, the asymmetry is a more extended structural property, which depends on the relative difference of environments in the two wells of Figure 4(b). These environments will tend to arrange themselves so as to minimise the energy. For this reason, it is reasonable to find that the values of Δ_c are rather small compared to V_0 in such a strong network glass.

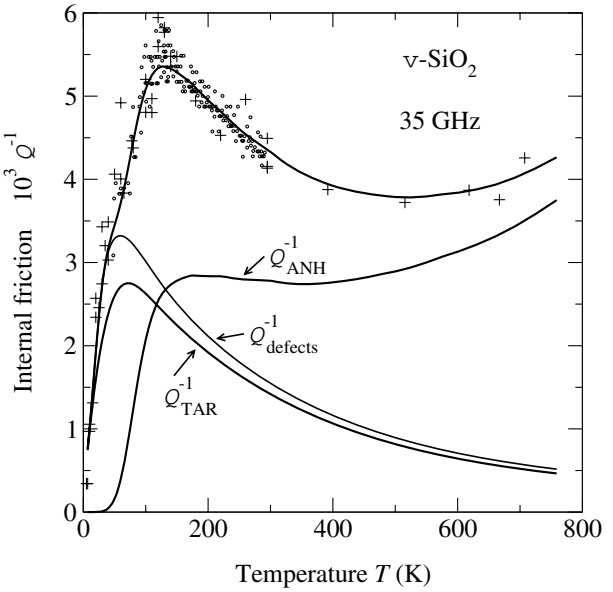

Figure 6. Internal friction of v-SiO_2 at hypersonic frequencies on the longitudinal acoustic mode, from Ref. 16. The lines show the defect relaxation contribution, which is mainly Q_{TAR}^{-1}, and the distinct anharmonic contribution

From Section 2, one should expect that at frequencies Ω well above ultrasonic ones, anharmonicity might start playing a role. Indeed, from Equation (5), Q_{TAR}^{-1} near the maximum of its peak is nearly independent of Ω since the last factor within parentheses just equals then ≈½. In contrast, in the same T-region, anharmonicity still is in the regime $\Omega\tau_{th} \ll 1$, so that the corresponding $Q^{-1} \propto \Omega$. This is illustrated for v-SiO_2 in Figure 6. The data is the Q^{-1} measured in BLS at 35 GHz.[16,19,23] It is compared to the Q_{TAR}^{-1} calculated with the above parameters, and to which a small contribution from two level systems[16] was added giving the total contribution of relaxing defects, $Q_{defects}^{-1}$. The difference, also shown, is the anharmonic contribution, labelled Q_{ANH}^{-1}, so that $Q^{-1} = Q_{defects}^{-1} + Q_{ANH}^{-1}$. Clearly, at sufficiently high Ω and T, Q_{ANH}^{-1} dominates over Q_{TAR}^{-1}.

This is not unique to v-SiO_2. Figure 7 illustrates the case of vitreous germania, v-GeO_2.[24] In Figure 7(a) the internal friction, including the BLS data, was adjusted to TAR alone. This can approximately be done, as shown by the lines, but it grossely overestimates the TAR contribution to the velocity, as noticed by the authors themselves. This is shown in Figure 7(b), where the points are the measured BLS data, while the line is calculated from TAR alone using the fit parameters derived from the adjustments in Figure 7(a). Clearly, the BLS data in Figure 7(a) must contain an appreciable contribution from anharmonicity. For that reason, TAR has been overestimated, leading to the disagreement in Figure 7(b). Unfortunately, the restricted number of experimental results on germania does not allow producing yet a detailed analysis similar to the one that could be performed on v-SiO_2.[16]

Finally, we point out that there are glasses in which TAR is very small. One case is densified silica glass, d-SiO_2. This material is obtained by a treatment at elevated hydrostatic pressure and temperature.[25] The resulting glass reaches the density of crystal quartz, q-SiO_2, and it remains metastable for extremely long times at ambient pressure and temperatures up to several hundred degrees C. Figure 8 illustrates the hypersonic properties of d-SiO_2 obtained by BLS.[26] The internal friction in Figure 8(a) is strongly reduced compared to that of v-SiO_2. As shown in Figure 8(b), the sound velocity increases compared to that of v-SiO_2. The T-dependence reveals that the dip in the low-T region of the velocity, which is characteristic of TAR, disappeared from the d-SiO_2 data. Hence, d-

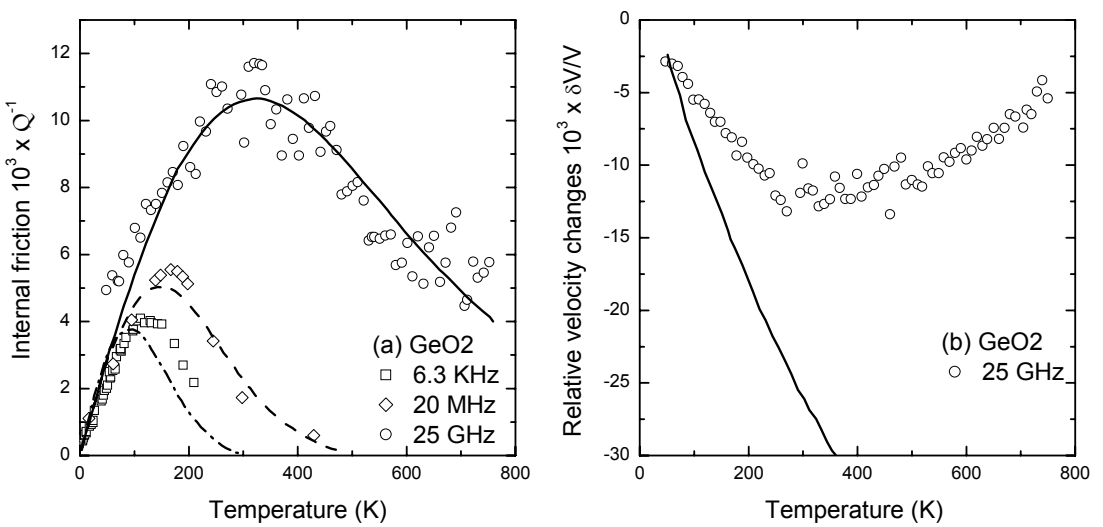

Figure 7. (a) Sonic, ultrasonic, and hypersonic damping results in vitreous germania adjusted to TAR alone[24] as shown by the lines; (b) the experimental and calculated velocity changes in the hypersonic regime, showing the strong disagreement which presumably results from neglecting anharmonicity

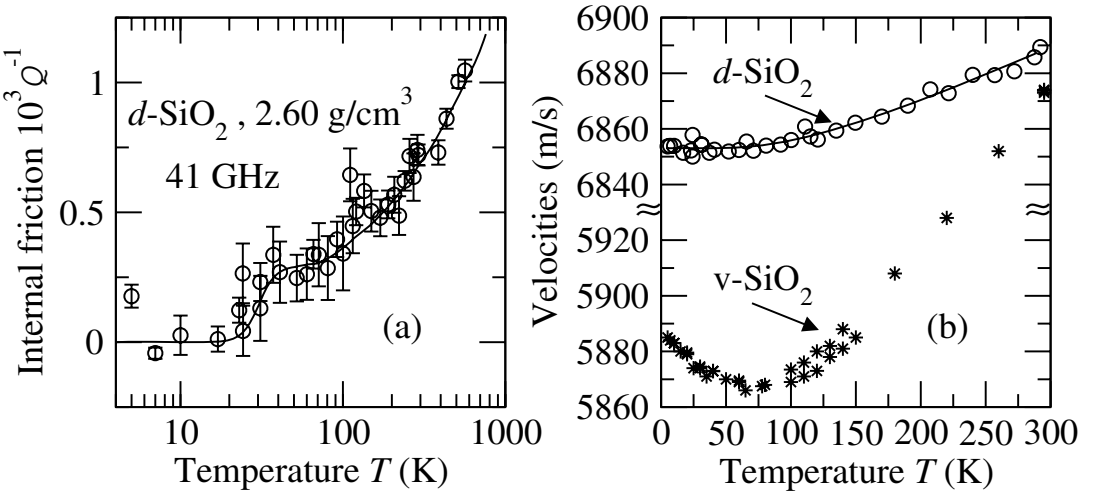

Figure 8. Internal friction (a) and sound velocity (b) of densified silica measured by Brillouin scattering, after Ref. 26. In (b), the velocity of normal vitreous silica is also shown for comparison

SiO_2 is an exceptional glass in which the contribution of anharmonicity alone can be investigated. Adjusting Q^{-1} with Equation (1) leads to the solid line in Figure 8(a). The strong reduction of TAR can be intuitively understood in terms of the model pictured in Figure 4(a). Densification eliminates to a large extent the free volume, preventing the formation of many deep double well potentials. This result is also confirmed by independent sonic measurements.[27]

4. Further understanding of silica and other strong glasses

4.1 Temperature hardening of vitreous silica

As described above, there are two main dynamical origins for sound velocity changes in glasses. Using the parameters of silica, these two contributions can be calculated in function of Ω and T, as shown in Figure 9(a).[16] Subtracting δv from v, one obtains the "unrelaxed" velocity v_∞. The result is illustrated in Figure 9(b), both for v-SiO_2 and d-SiO_2.[16] A remarkable property is that v_∞ is a growing function of T, having quantitatively similar shapes in both glasses. The only reasonable explanation for this behaviour is that there is a progressive structural change that occurs in silica as the temperature is raised. Contrary to TAR, this change is insensitive to densification. A similar behaviour is also found in other tetrahedrally coordinated glasses, including the non-oxide BeF_2.[18]

A possible explanation is related to the $\alpha \leftrightarrow \beta$ transformation of cristobalite, another cristalline form of silica. The transformation is due to cooperative rotations of Si–O–Si bridges.[28] The α-phase has a smaller density but a larger bulk modulus than the β-phase, as shown in Figure 10. This is a sizeable effect. Should something of this type occur as function of T in the glasses, it can well account for the experimental magnitudes in Figure 9(b). Such spontaneous modifications have been observed in numerical simulations of silica. The authors call it a "local progressive polyamorphic transition".[28]

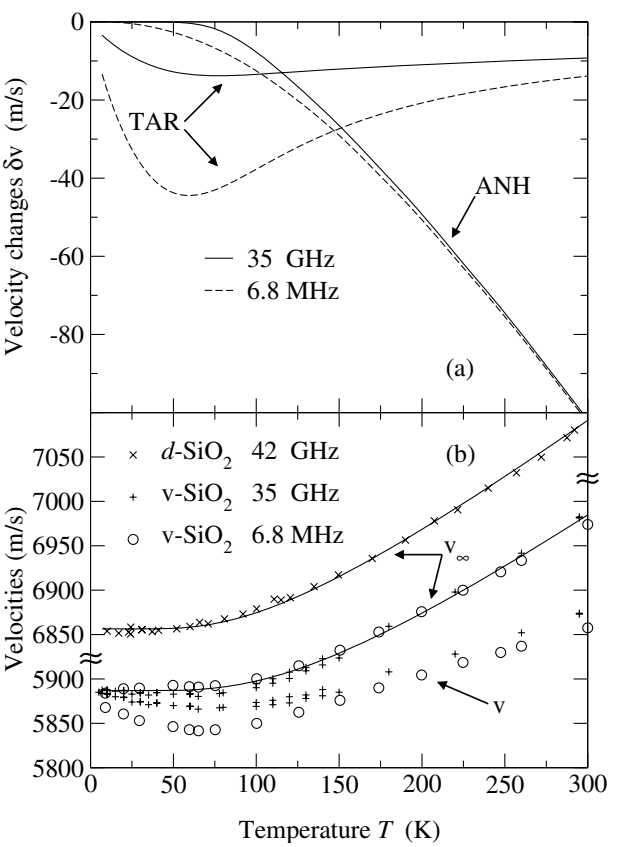

Figure 9. (a) The velocity changes of v-SiO_2 produced by TAR and anharmonicity, at two frequencies. (b) The velocities of the longitudinal mode of v-SiO_2, with (v) and without (v_∞) the contributions of the two relaxation processes, TAR and ANH. The velocity of the same unrelaxed mode is also shown for d-SiO_2, for comparison

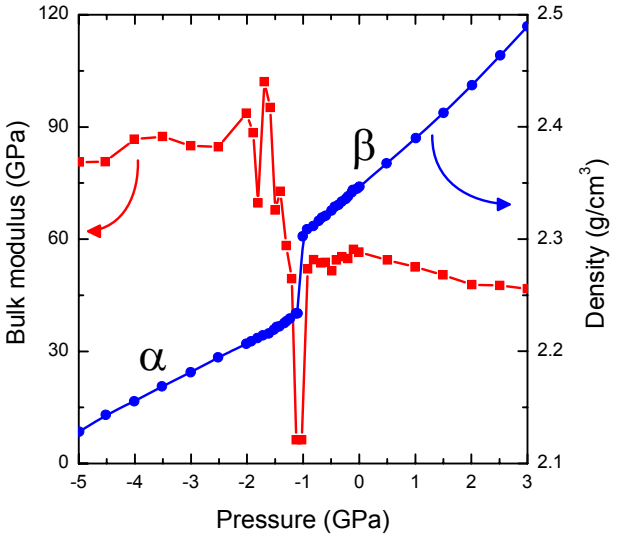

Figure 10. Simulation results on the bulk modulus and density of cristobalite obtained by variation of the hydrostatic pressure. The less compact α phase has also a much higher modulus and therefore a higher sound velocity. After Ref. 28

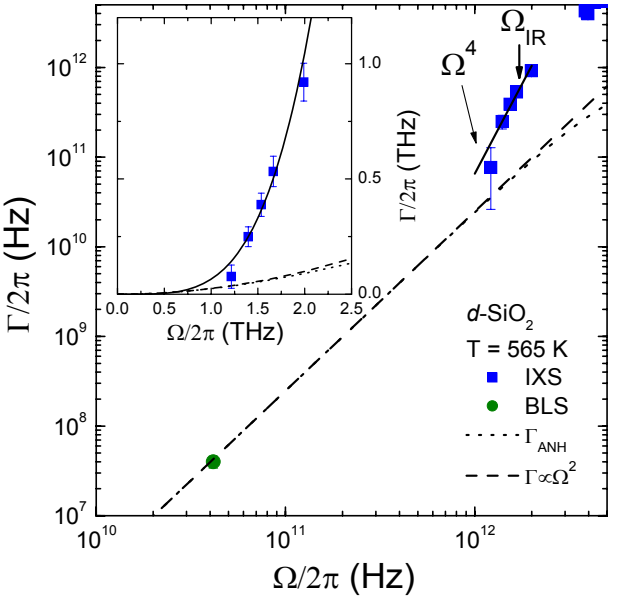

Figure 11. IXS results on the linewidth of the longitudinal acoustic modes in d-SiO_2, showing the region of Ω^4 broadening below Ω_{IR}, from Ref. 30. These points lie well above the extrapolated anharmonic contribution, as emphasised on the linear scale of the inset which also shows the experimental error bars on the data points. The lines are explained in the text

4.2 Thermal conductivity and the Ioffe–Regel crossover

For reasons explained in Section 2.3, it is of interest to study sound waves up to very high Ω. For several processes, such as anharmonicity, the linewidth Γ increases faster than Ω. One might thus expect that at some stage, as Ω increases, one could reach a point where the sound wavelength λ_s becomes equal to the mean free path for the sound amplitude, which equals 2*l*. This is called the Ioffe–Regel (IR) limit[29] beyond which the wavevector **q** has lost its meaning. At and above this Ioffe–Regel frequency Ω_{IR}, plane waves do not exist anymore and sound becomes a diffuse excitation. With $l=\lambda_s/2$, and since $\lambda_s=2\pi v/\Omega$ and $\Gamma=v/l$, one finds for the IR-limit the relation $\Gamma_{IR}=\Omega_{IR}/\pi$.

In two favourable cases it was possible to study the approach of Ω_{IR} from below using Brillouin scattering of x-rays with IXS. Results obtained on d-SiO_2[30] are illustrated in Figure 11. The dashed line is the law $\Gamma \propto \Omega^2$ extrapolated from the BLS measurement shown in Figure 8. The dotted line is the anharmonic contribution calculated from Equation (1). In the region of the IXS measurement, the simple Ω^2 extrapolation starts slowly breaking down. On the other hand, the observed linewidths are much larger than just the anharmonic contribution. In fact Γ in this region shows a dramatic increase, $\Gamma \approx \Omega^4$, which indicates a new mechanism, different from TAR and anharmonicity. This rapidly produces the IR crossover at the place indicated by the arrow. Such a rapid increase in Γ(Ω) is precisely what is required[31] to produce the plateau in κ(*T*) at $k_B T_p \approx \hbar\Omega_{IR}/5$. With $\Omega_{IR}/2\pi$=1·7 THz in d-SiO_2, this gives T_p≈17 K, in agreement with an independent measurement of κ.[32]

The second example for which a law $\Gamma \approx \Omega^4$ could be observed with IXS is a lithium borate glass, Li_2O–$2B_2O_3$,[33] as shown in Figure 12. In that case, contrary to d-SiO_2, TAR continues to be an important mechanism in optical BLS. It produces the dependence $\Gamma \approx \Omega$ shown by the dashed line. The line labelled Γ_{ANH} is a rough estimate of the anharmonic linewidth contribution. The rapid increase, measured with IXS, is shown by the line $\Gamma \approx \Omega^4$. The IR-crossover, at $\Omega_{IR}/2\pi$=2·1 THz, is shown by the arrow. This would predict T_p≈20 K for this glass. The corresponding data on κ are not yet available.

It is of course of immediate interest to understand the origin of the rapid increase $\Gamma \propto \Omega^4$ leading to Ω_{IR}. There exist in glasses vibrational modes of low frequency that are in excess over the acoustic modes. These show up in plots of $g(\omega)/\omega^2$, where $g(\omega)$ is the vibrational density of states (DOS). Acoustic modes contribute a "Debye density of states", $g_D(\omega)/\omega^2$, which is the one observed up to fairly high frequencies in crystals.[12] In most glasses, the reduced DOS, $g(\omega)/\omega^2$, exhibits a peak above the horizontal line $g_D(\omega)/\omega^2$ calculated from the velocities of the sound waves. This excess, located at Ω_{BP}, is called the boson peak (BP). It also produces in the specific heat an excess over the Debye value.[34] The BP appears in various spectroscopies, Raman, hyper-Raman, neutron, and x-ray scatterings. Of course, the observed BP in these spectroscopies might vary, depending on the coupling of the DOS with the particular probe. It

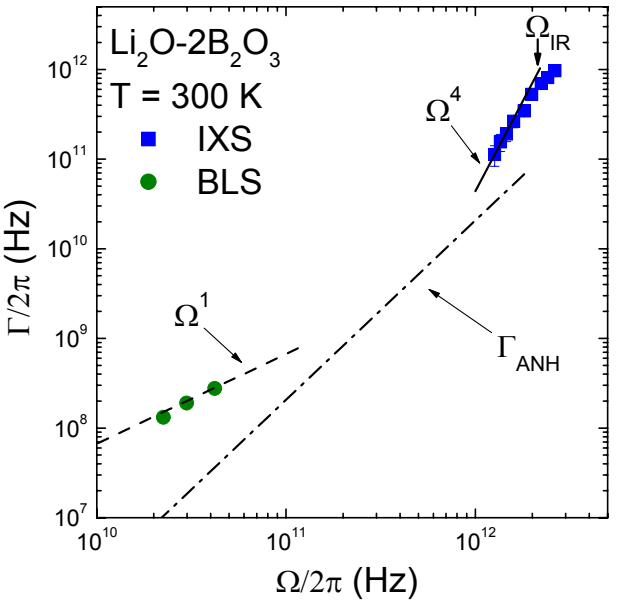

Figure 12. IXS and Brillouin light scattering linewidths of the longitudinal acoustic mode of lithium diborate showing the rapid onset of the broadening in the THz region, from Ref. 33. The lines are explained in the text

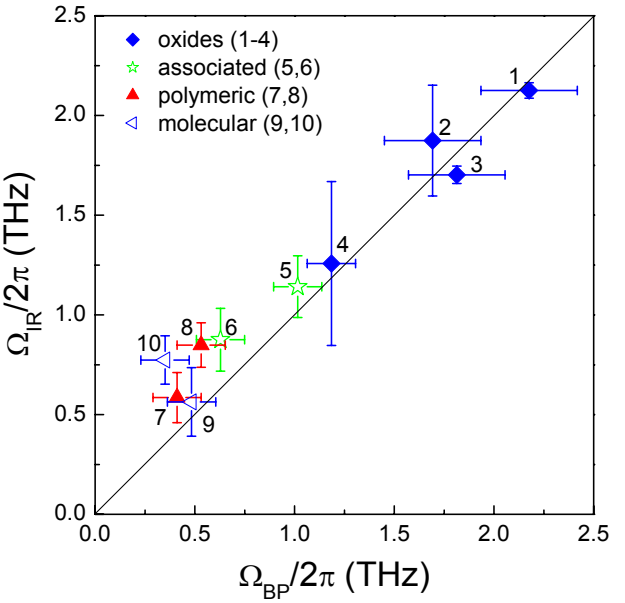

Figure 13. The relation between IR and BP for various glasses. The points are: (1) lithium diborate, Li_2O–$2B_2O_3$ at 573 K; (2) lithium tetraborate, Li_2O–$4B_2O_3$; (3) densified silica, d-SiO_2 at 565 K; (4) vitreous silica, v-SiO_2 at ~1050 K; (5) glycerol at 175 K; (6) ethanol at 86 K; (7) selenium at 295 K; (8) polybutadiene at 140 K; (9) propylene carbonate at 167 K (T_g+7 K); (10) orthoterphenyl (OTP) at 156 K. The line $\Omega_{IR}=\Omega_{BP}$ is a guide to the eye. The error bars on Ω_{IR} are explained in Ref. 37, those on Ω_{BP} in Ref. 38

is remarkable that for the above two examples, one finds $\Omega_{IR}\approx\Omega_{BP}$. This strongly suggests that the rapid increase of Γ and the location of the BP are related. In fact, one should expect a hybridisation between the sound wave modes and the excess modes, which reconstructs the DOS, as explained in Refs 35, 36. This appears today as the most reasonable explanation for the remarkable coincidence of the IR-crossover, the boson peak, and the thermal conductivity plateau.

It is thus of interest to check whether $\Omega_{IR}\approx\Omega_{BP}$ occurs in other cases. Although the region below Ω_{IR} could only be investigated so far for the above two examples, there is sufficient data in the recent literature to estimate IR for a collection of glasses. The procedure has been explained elsewhere.[37] It leads to the coincidence shown in Figure 13. The large error bars on Ω_{BP} result from the uncertainty in the exact position of the peak in the reduced DOS. Ideally, the Ω_{BP} for this comparison should probably be derived from low *T* specific heats,[38] but the needed data are mostly not available. Figure 13 shows, beyond doubts, that Ω_{IR} and Ω_{BP} are related. The figure includes four network glasses for which one nearly finds $\Omega_{IR}=\Omega_{BP}$. These are all strong glasses in the sense of Angell[39] which are known to have relatively large excesses of modes.[40] There is also data for two associated glass formers, glycerol and ethanol. Glycerol is a strongly associated liquid and the corresponding data point in Figure 13 nearly reaches the region of the network glasses. Ethanol is also an associated glass former, but it only forms chains.[41] This is similar for the two polymeric glasses for which we have data, the inorganic polymer selenium, and the organic one, polybutadiene. These are not rigid glasses in the sense of Thorpe.[42] Their data points in Figure 13 fall in the same region as for the two molecular glasses. The latter are fragile systems in the sense of Angell.[39] In the latter five cases it seems that Ω_{IR} is somewhat larger than Ω_{BP}, although the two frequencies still appear to be related. A similar observation of a relation between Ω_{IR} and Ω_{BP} was already presented in Ref. 43, not based on measured values of Ω_{IR} but on calculated ones using the soft potential model.[44]

5. Conclusions

In this review, it is shown that there are major differences between the acoustical properties of crystals and glasses. In the case of glasses, we identified three mechanisms that contribute to sound attenuation. In order of increasing frequency, these are the thermal relaxation of local defects, the relaxation via anharmonic interactions with the thermal bath, and the hybridisation with excess low frequency optic like vibrations. This allows describing the sound damping over more than nine orders of magnitude in frequencies, from the kHz to the THz. These mechanisms, which are frequency and temperature dependent, contribute not only to sound damping but also to velocity changes. The information derived from the

latter is particularly valuable as it integrates differently over the distribution of relaxations. In addition, measurements of velocity changes in function of temperature reveal that in tetrahedrally coordinated glasses there occurs progressive structural changes which produce hardening as the temperature is raised.

At very high frequencies, in the THz range, sound changes its nature, becoming diffusive rather than wavelike. This Ioffe–Regel crossover nearly coincides with the excess of vibrational modes manifested by the boson peak. This strongly suggests that the Ioffe–Regel crossover is produced by the hybridisation of acoustic and optic modes. The crossover also accounts for the existence and location of a plateau in the temperature dependence of the low temperature thermal conductivity.

Acknowledgements

Many thanks are addressed to Dr Giulio Monaco at the ESRF, Grenoble, France, for the fruitful collaboration that has led to the IXS results presented in Figures 11 and 12. Appreciation is expressed to Rémy Vialla for the BLS instrumental improvements that allowed obtaining high resolution data such as those presented in Figure 8.

References

1. Maris, H. J. *Physical Acoustics*, 1971, Vol. VIII, pp. 279–345. Edited by W. P. Mason & R. N. Thurston, Academic Press, New York.
2. Claytor, T. N. & Sladek, R. J. *Phys. Rev. B*, 1978, **18**, 5842.
3. Vacher, R., Pelous, J., Plicque, F. & Zarembowitch, A. *J. Non-Cryst. Solids*, 1981, **45**, 397.
4. Anderson, O. L. & Bömmel, H. E. *J. Am. Ceram. Soc.*, 1955, **38**, 125.
5. Hunklinger, S. & Arnold, W. *Physical Acoustics*, 1976, Vol. XII, pp. 155–215. Edited by W. P. Mason & R. N. Thurston, Academic Press, New York.
6. Masciovecchio, C., Gessini, A., Di Fonzo, S., Comez, L., Santucci, S. C. & Fioretto, D. *Phys. Rev. Lett.*, 2004, **92**, 247401.
7. Benassi, P., Caponi, S., Eramo, R., Fontana, A., Giugni, A., Nardone, M., Sampoli, M. & Viliani, G. *Phys. Rev. B*, 2004, **71**, 172201.
8. Vacher, R., Ayrinhac, S., Foret, M., Rufflé, B. & Courtens, E. *Phys. Rev. B*, 2006, **74**, 012203.
9. Sette, F., Krisch, M. H., Masciovecchio, C., Ruocco, G. & Monaco, G. *Science*, 1998, **280**, 1550.
10. Zhu, T. C., Maris, H. J. & Tauc, J. *Phys. Rev. B*, 1991, **44**, 4281.
11. Zeller, R. C. & Pohl, R. O. *Phys. Rev. B*, 1971, **4**, 2029.
12. Kittel, C. *Introduction to Solid State Physics*, 1967, Third ed., Wiley, New York.
13. Akhiezer, A. *J. Phys. (USSR)*, 1939, **1**, 227.
14. Bömmel, H. E. & Dransfeld, K. *Phys. Rev.*, 1960, **117**, 1245.
15. Blinick, J. S. & Maris, H. J. *Phys. Rev. B*, 1970, **2**, 2139.
16. Vacher, R., Courtens, E. & Foret, M. *Phys. Rev. B*, 2005, **72**, 214205.
17. Landau, L. D. & Lifshitz, E. M. *Electrodynamics of Continuous Media*, 1967, Pergamon Press, Oxford.
18. Krause, J. T. & Kurkjian, C. R. *J. Am. Ceram. Soc.*, 1968, **51**, 226.
19. Tielbürger, D., Merz, R., Ehrenfels, R. & Hunklinger, S. *Phys. Rev. B*, 1992, **45**, 2750.
20. Jäckle, J., Piché, L., Arnold, W. & Hunklinger, S. *J. Non-Cryst. Solids*, 1976, **20**, 365.
21. Phillips, W. A. *Rep. Prog. Phys.*, 1987, **50**, 1657.
22. Keil, R., Kasper, G. & Hunklinger, S. *J. Non-Cryst. Solids*, 1993, **164–166**, 1183.
23. Vacher R. & Pelous, J. *Phys. Rev. B*, 1976, **14**, 823.
24. Hertling, J., Baeßler, S., Rau, S., Kasper, G. & Hunklinger, S. *J. Non-Cryst. Solids*, 1998, **226**, 129.
25. Bridgman, P. W. & Šimon, I. *J. Appl. Phys.*, 1953, **24**, 405.
26. Rat, E., Foret, M., Massiera, G., Vialla, R., Arai, M., Vacher, R. & Courtens, E. *Phys. Rev. B*, 2005, **72**, 214204.
27. Weiss, G., Daum, A., Sohn, M. & Arndt, J. *Physica B*, 1996, **219&220**, 290.
28. Huang, Liping & Kieffer, J. *Phys. Rev. B*, 2004, **69**, 224203 & 224204.
29. Ioffe A. F. & Regel, A. R. *Prog. Semicond.*, 1960, **4**, 237.
30. Rufflé, B., Foret, M., Courtens, E., Vacher, R. & Monaco, G. *Phys. Rev. Lett.*, 2003, **90**, 095502.
31. Randeria, M. & Sethna, J. *P. Phys. Rev. B*, 1988, **38**, 12607.
32. Zhu, Da-Ming *Phys. Rev. B*, 1994, **50**, 6053.
33. Rufflé, B., Guimbretière, G., Courtens, E., Vacher, R. & Monaco, G. *Phys. Rev. Lett.*, 2006, **96**, 045502.
34. Buchenau, U., Prager, M., Nucker, N., Dianoux, A. J., Ahmad, N. & Phillips, W. A. *Phys. Rev. B*, 1986, **34**, 5665.
35. Gurevich, V. L., Parshin, D. A. & Schober, H. R. *Phys. Rev. B*, 2003, **67**, 094203.
36. Klinger, M. I. & Kosevich, A. M. *Phys. Chem. Glasses*, 2003, **44**, 187.
37. Courtens, E., Rufflé, B. & Vacher, R. *J. Neutron Res.*, 2006, **13**, 361.
38. Rufflé, B., Guimbretière, G., Courtens, E., Vacher, R. & Monaco, G. *Phys. Rev. Lett.*, 2007, **98**, 079602.
39. Angell, C. A. *J. Non-Cryst. Solids*, 1991, **131–133**, 13.
40. Sokolov, A. P., Rössler, E., Kisliuk, A. & Quitmann, D. *Phys. Rev. Lett.*, 1993, **71**, 2062.
41. Saiz, L., Padró, J. A. & Guàrdia, E. *J. Phys. Chem. B*, 1997, **101**, 78.
42. Thorpe, M. F. *J. Non-Cryst. Solids*, 1983, **57**, 355.
43. Parshin, D. A. & Laermans, C. *Phys. Rev. B*, 2001, **63**, 132203.
44. Karpov, V. G., Klinger, M. I. & Ignatíev, F. N. *Sov. Phys. JETP*, 1983, **57**, 439. For a review see Parshin, D. A. *Phys. Solid State*, 1994, **36**, 991.